Supporting Information

Spring-like fiber based strain sensor with fast response and high sensitivity for precise detection of complicated human activities

Yunjian Zhu, Jiahao Liu, Manman Ou, Leyu Dai, Weiwei Zhang, Jianjun Wang, Jun Sun, * Chuanxiang Qin* and Lixing Dai*

College of Chemistry, Chemical Engineering and Materials Science, Soochow University, Suzhou 215123, P. R. China.
Corresponding author E-mail: dailixing@suda.edu.cn; qinchuanxiang@suda.edu.cn; sunjun@suda.edu.cn

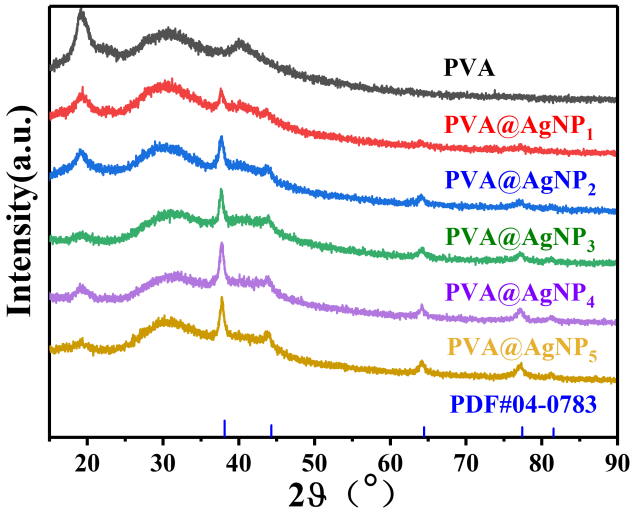

Figure S1. XRD images of PVA fiber and PVA@AgNP$_x$ fibers, and XRD standard card of nanosilver (PDF#04-0783). It can be clearly found that the nanosilver characteristic peak intensity of PVA@AgNP$_x$ fiber is increasing with the increase of the cycles of silver precursor adsorption and hydrazine reduction.

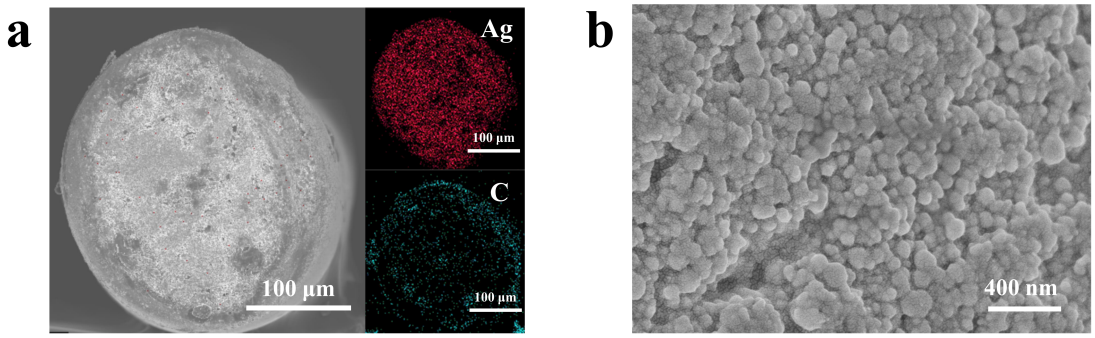

Figure S2. (a) Cross-sectional SEM image of PVA@AgNP$_5$ fiber and its EDS mapping images of Ag and C. (b) Enlarged morphology of PVA@AgNP$_5$ fiber cross-section.

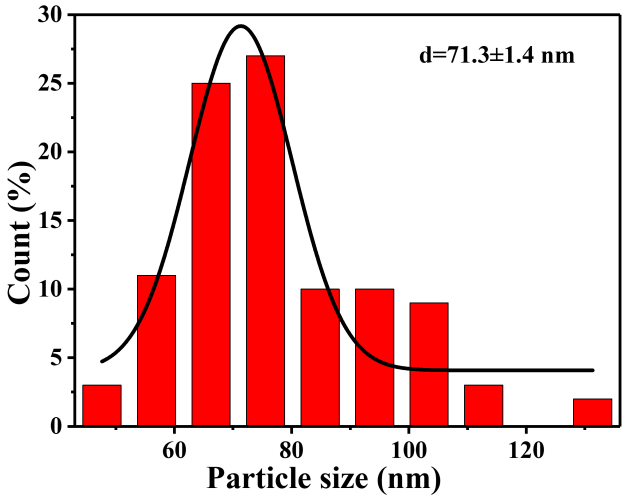

Figure S3. Diameter distribution of AgNP in the cross-section of PVA@AgNP$_5$ fiber.

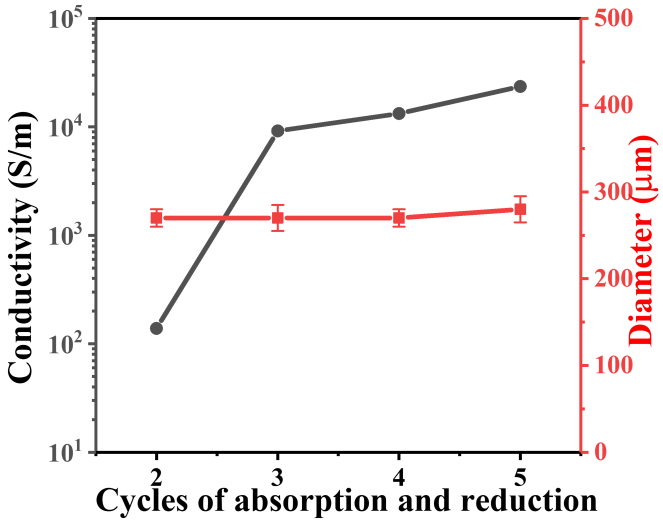

Figure S4. Conductivity and diameter of PVA@AgNP$_x$ fiber at different cycles of absorption and reduction.

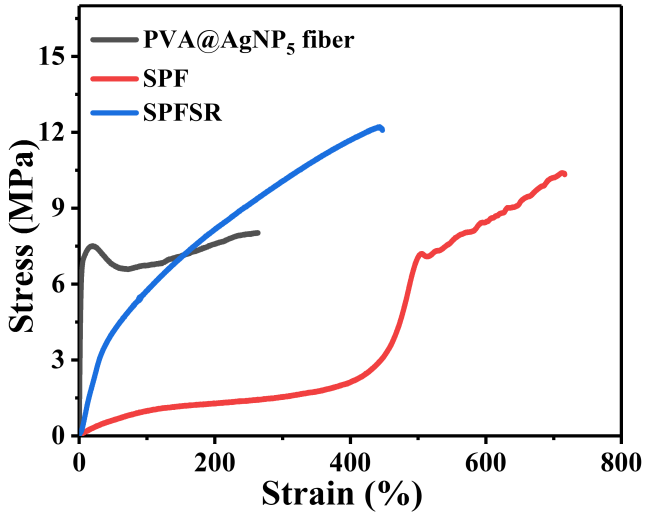

Figure S5. Stress-strain curves of the original and spring-like PVA@AgNP$_5$ fibers (SPF) and the strain sensor (SPFSR).

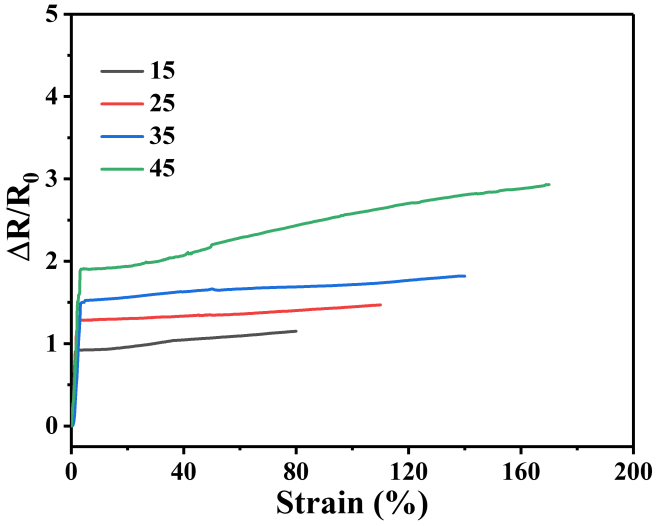

Figure S6. Relationship between $\Delta R/R_0$ and strain of SPFSR with 15, 25, 35, and 45 helixes stretched to R-strain$_{max}$ at a strain rate of 50 mm/min.

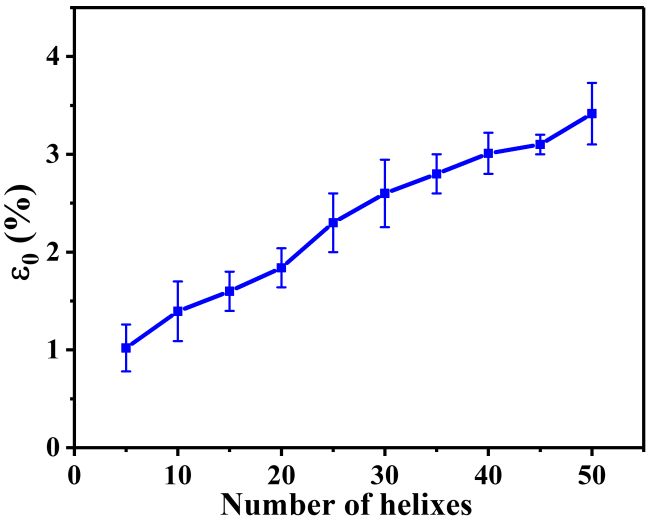

Figure S7. The ε_0 of SPFSR with different number of helixes.

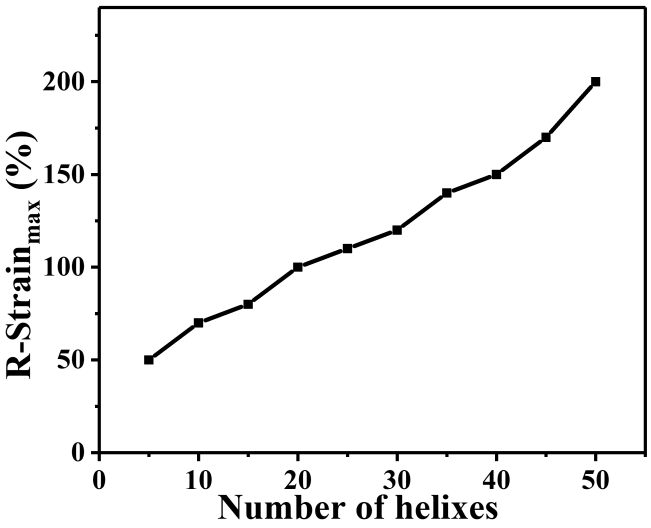

Figure S8. The variations of R-strain$_{max}$ of SPFSR with different number of helixes. R-strain$_{max}$ of the sensor increases significantly with the increasing number of helixes.

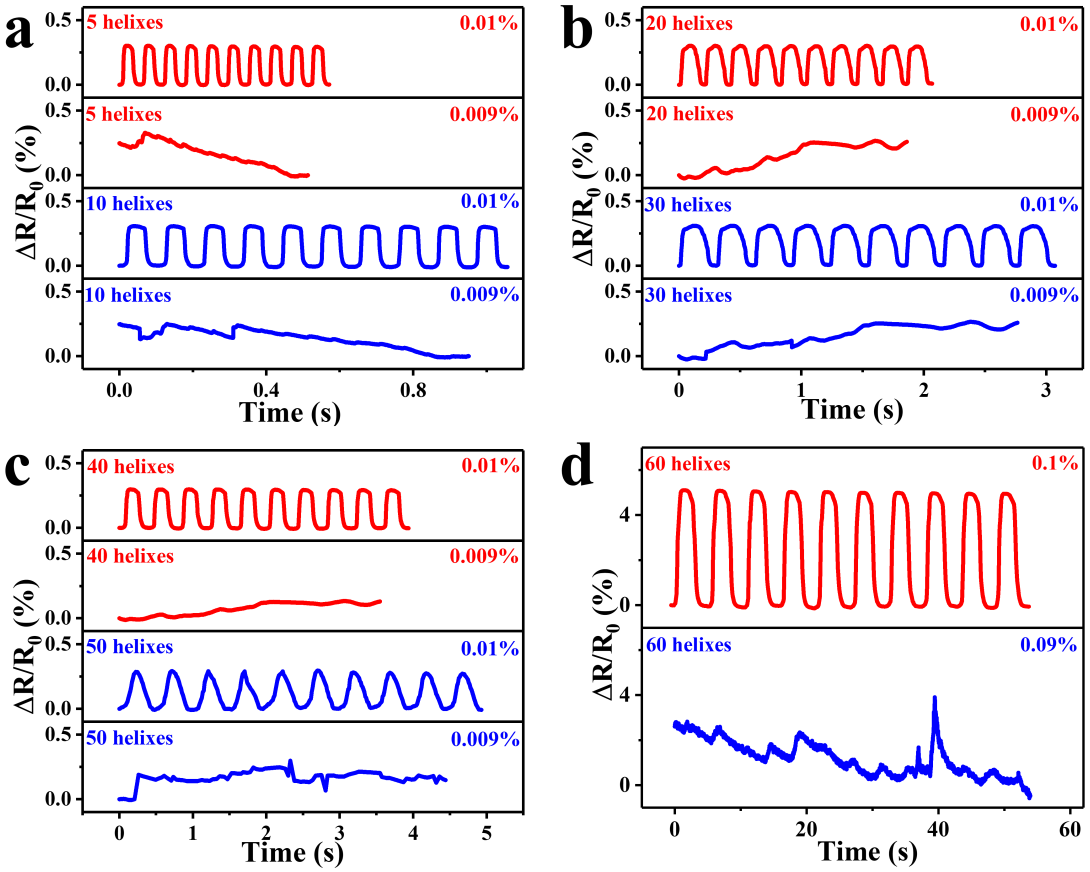

Figure S9. The response curves of SPFSR with (a) 5, 10, (b) 20, 30 (c) 40, 50 helixes in 10 cycles at strains of 0.01% and 0.009%. (d) The response curves of SPFSR with 60 helixes in 10 cycles at strains of 0.1% and 0.09%. All the above tests were carried out at a strain rate of 1 mm/min. SPFSR with less than 50 helixes have a stable response to 0.01% strain, but cannot response to 0.009% strain (Figure S9a-c). SPFSR with 60 helixes has a stable response to 0.1% strain, but cannot response to 0.09% strain (Figure S9d). Thus, the sensors with the helixes less than 50 can reach an extremely low detection limit of strain 0.01%.

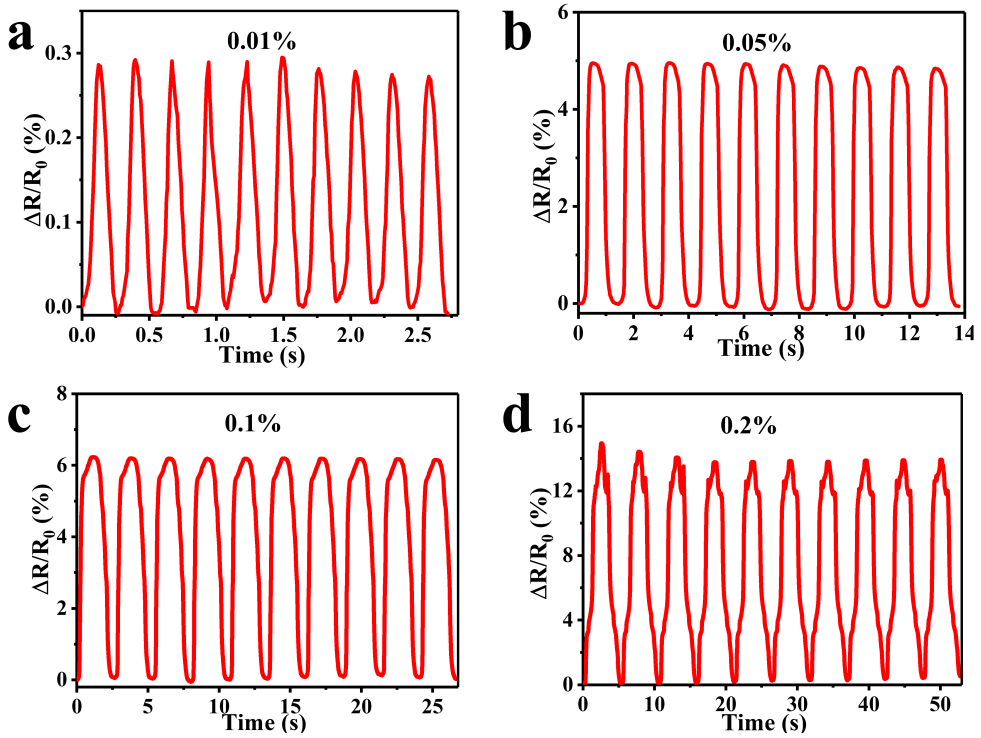

Figure S10. The response curves of the sensor in 10 cycles at (a) 0.01%, (b) 0.05%, (c) 0.1%, and (d) 0.2% strain at a strain rate of 2 mm/min.

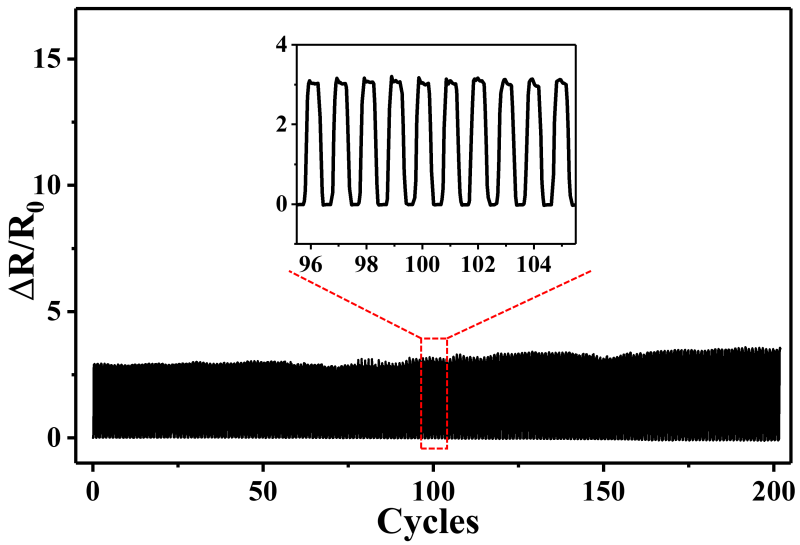

Figure S11. The response curve of the sensor with cyclic stretching 100% strain for 200 times at a strain rate of 500 mm/min.

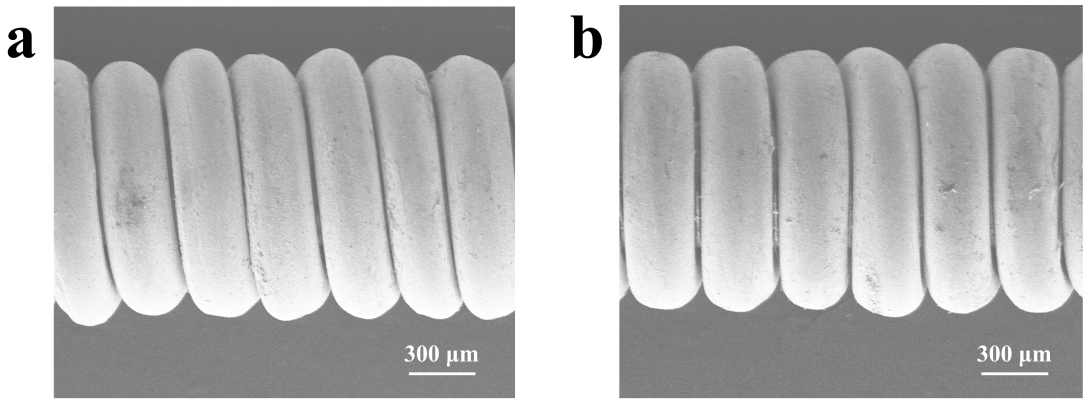

Figure S12. SPFSR after (a) 5000 and (b) 12000 stretching−releasing cycles at a strain of 10% at a strain rate of 500 mm/min.

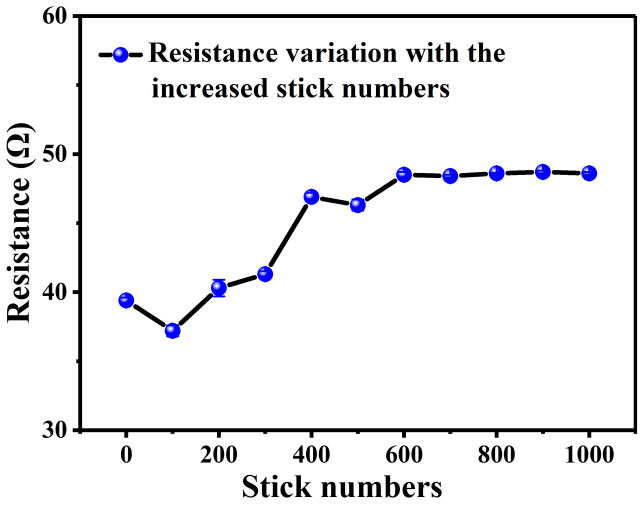

Figure S13. Resistance variation of PVA@AgNP$_5$ fiber after being stuck and stripped for 1000 cycles by tapes.

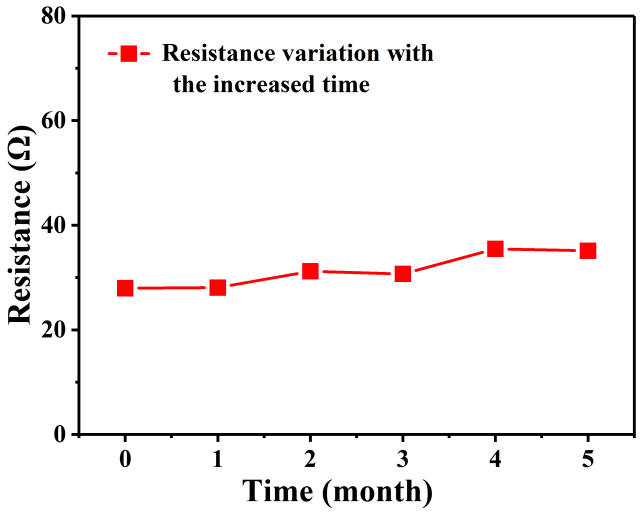

Figure S14. Resistance variation of a PVA@AgNP$_5$ fiber in 5 months in ambient environment.

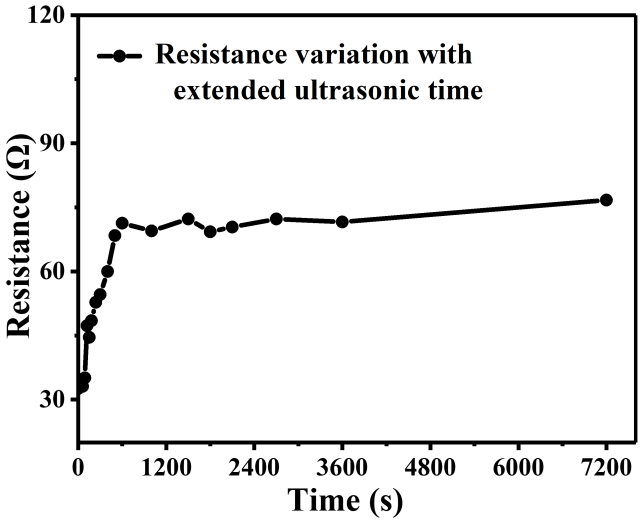

Figure S15. Resistance variation of a PVA@AgNP$_5$ fiber with extended ultrasonic time.

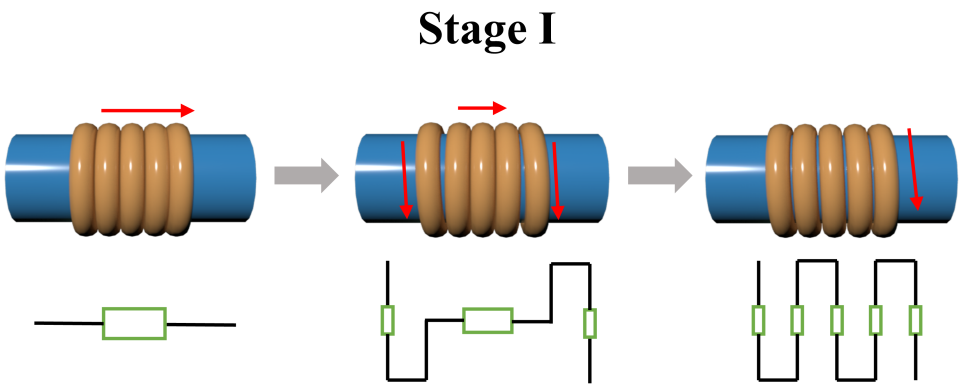

Figure S16. Schematic illustration of the sensing mechanism of the sensor in stage I.

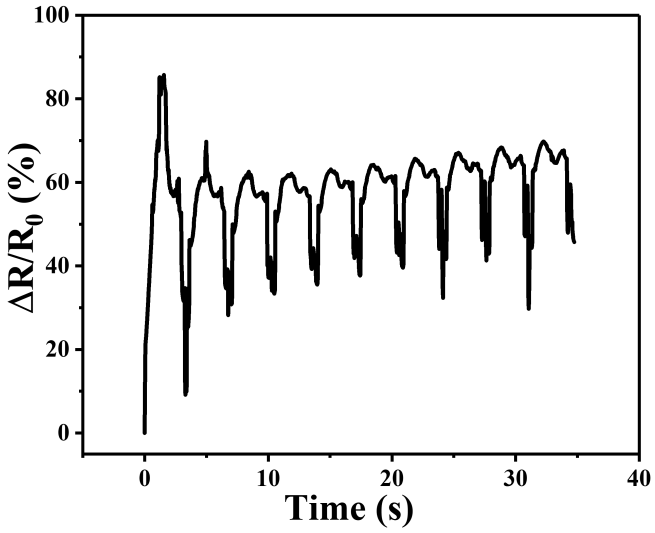

Figure S17. *ΔR/R₀* curve of SPFSR during 10 bending-releasing cycles at *ΔL/L₀* of 60% at a strain rate of 600 mm/min.

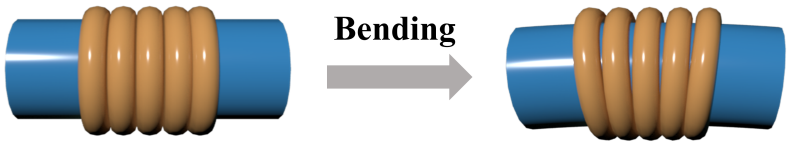

Figure S18. Schematic illustration of the sensor from the original to the bending state.

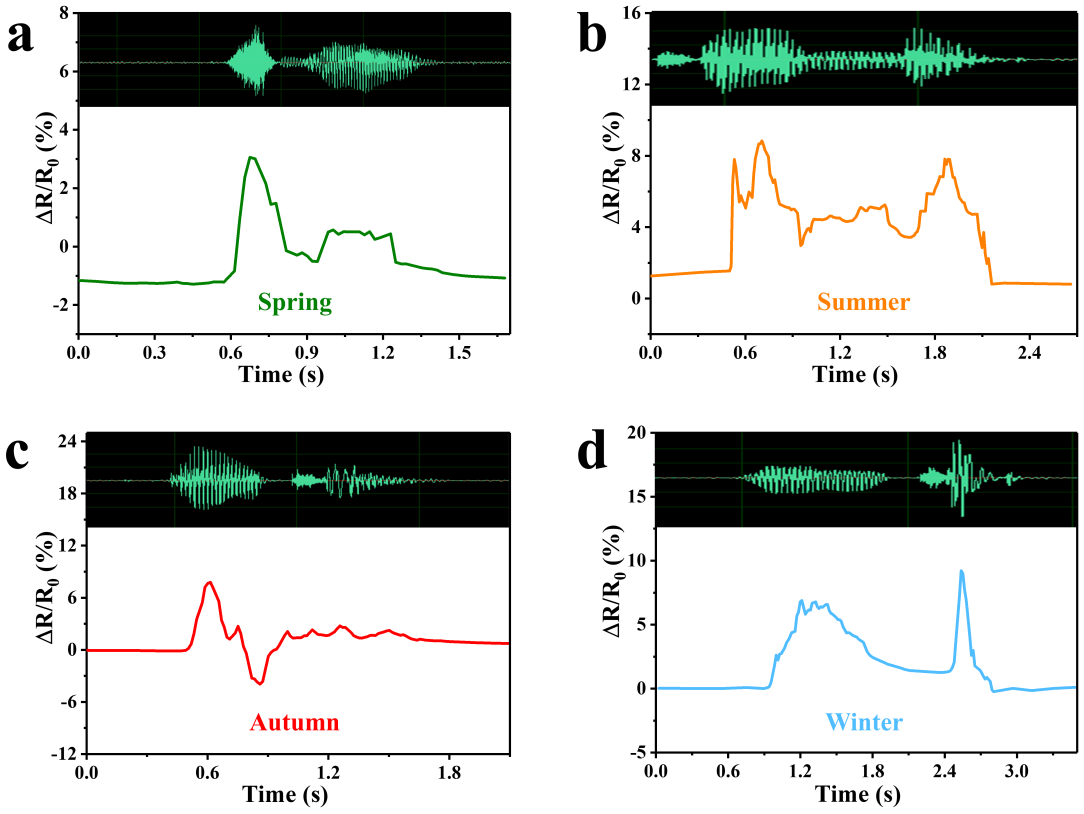

Figure S19. The response curves (lower) of the sensor and the corresponding sound wave diagram (upper) of the word (a) "Spring", (b) "Summer", (c) "Autumn", and (d) "Winter" pronounced once.

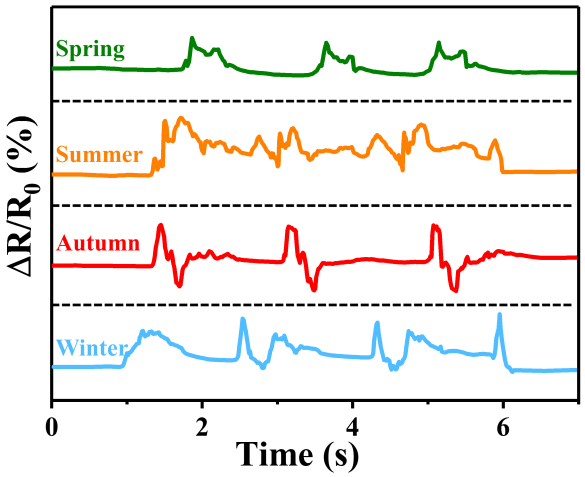

Figure S20. The response curves of the sensor when pronouncing the word "Spring", "Summer", "Autumn" and "Winter" three times continuously.

Figure S21. The sensor is attached to the chest and marked in the red box.

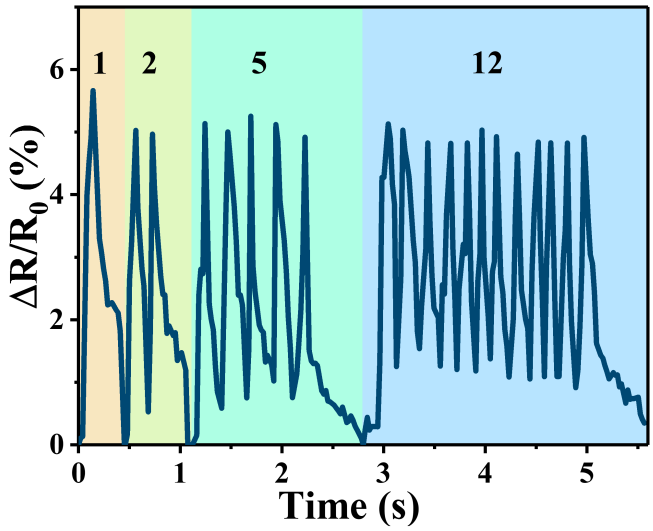

Figure S22. The response curve of the sensor to 1, 2, 5, and 12 knocks during different times.

Table S1. Key parameters of the reported similar types of strain sensors

Ref.	Materials	Sensitivity	Detection range	Response time
1	Graphene PE and PU (core)	10(1%) 3.7(50%)	0.2%-100%	100 ms
2	Carbon link Elastic core-spun yarn	6.1(0.5%-20%)	0.5%-100%	110 ms
3	CNT PP and Rubber (core)	2.21(0%-200%)	0.01%-200%	70 ms
4	CNT Cotton and PU (core)	0.82(0%-40%) 0.06(60%-200%)	1%-300%	>200 ms
5	AgNW Cotton and PU (core)	1.6(1%-50%) 4.7(50%-200%)	1%-200%	>200 ms
6	PAN/rGO Cotton and PU (core)	max=11(0.1%-200%)	0.1%-200%	100 ms
7	Mxene Helical core-sheath yarns	0.67(0.3%-100%)	0.3%-120%	120 ms
8	MWCNTs/rGO Core-spun yarn	3.34(0.1%-70%) 2.5(70%-200%) 3.7(200%-300%)	0.1%-300%	140 ms
9	PDA/CB Core-spun yarn	3.1(1%-150%) 1.7(150%-400%)	1%-400%	>200 ms
10	CB/Ag/CNT Core-spun yarn	2.18(0.5%-50%)	0.5%-50%	125 ms
11	Ppy/CNT Core-spun yarn	5.11(0.1%-50%) 3.41(50%-350%)	0.1%-350%	>200 ms
12	GO Core-spun yarn	1.5(0.3%-100%)	0.3%-100%	120 ms
13	carbon fiber PAN and Cotton(core)	37.3(0.1%) 11.5(0.3%-30%)	0.1%-30%	>200 ms
This work	AgNP PVA and Rubber (core)	66.32(0.01%-3.5%) 0.73(3.5%-200%)	0.01%-200%	42 ms

Notes and references

1. Y. Cheng, R. Wang, J. Sun and L. Gao, *Adv. Mater.*, 2015, **27**, 7365-7371.
2. Z. H. Duan, Y. D. Jiang, S. Wang, Z. Yuan, Q. N. Zhao, G. Z. Xie, X. S. Du and H. L. Tai, *Acs Sustain. Chem. Eng.*, 2019, **7**, 17474-17481.
3. L. Lu, Y. Zhou, J. Pan, T. Chen, Y. Hu, G. Zheng, K. Dai, C. Liu, C. Shen, X. Sun and H. Peng, *ACS Appl. Mater. Interfaces*, 2019, **11**, 4345-4352.
4. Z. F. Wang, Y. Huang, J. F. Sun, Y. Huang, H. Hu, R. J. Jiang, W. M. Gai, G. M. Li and C. Y. Zhi, *Acs Appl. Mater. Interfaces*, 2016, **8**, 24837-24843.
5. M. Zhao, D. W. Li, J. Y. Huang, D. Wang, A. Mensah and Q. F. Wei, *J. Mater. Chem. C*, 2019, **7**, 13468-13476.
6. W. Zhai, X. Y. Li, Q. J. Xia, P. F. Zhan, J. W. Xu, G. Q. Zheng, K. Dai, Z. C. Zhang, C. T. Liu and C. Y. Shen, *Compos. Part B-Eng.*, 2021, **211**, 108621.
7. L. H. Wang, M. W. Tian, Y. Y. Zhang, F. Q. Sun, X. J. Qi, Y. M. Liu and L. J. Qu, *J. Mater. Sci.*, 2020, **55**, 6187-6194.
8. M. Zhang, P. Feng, X. Lian, G. Zhao, C. Liu, N. Li, J. Xu, Y. Chen and X. Jian, *J. Appl. Polym.*, 2023, **140**, e54288.
9. M. C. Qu, D. W. Li, T. X. Qin, Z. Y. Luo, X. H. Liu, F. Nilsson, Q. Gao, Z. X. Zheng and Y. J. Qin, *Acs Appl. Nano Mater.*, 2022, **5**, 16996-17003.
10. P. Liu, W. D. Pan, Y. Liu, J. Liu, W. R. Xu, X. H. Guo, C. X. Liu, Y. G. Zhang, Y. J. Ge and Y. Huang, *Compos. Sci. Technol.*, 2018, **159**, 42-49.
11. G. Cai, B. Hao, L. Luo, Z. Deng, R. Zhang, J. Ran, X. Tang, D. Cheng, S. Bi, X. Wang and K. Dai, *ACS Appl. Mater. Interfaces*, 2020, **12**, 29717-29727.
12. L. Wang, M. Tian, X. Qi, X. Sun, T. Xu, X. Liu, S. Zhu, X. Zhang and L. Qu, *Langmuir*, 2021, **37**, 3122-3129.
13. T. Yan, H. Zhou, H. T. Niu, H. Shao, H. X. Wang, Z. J. Pan and T. Lin, *J. Mater. Chem. C*, 2019, **7**, 10049-10058.